







Adaptive estimation method for determining inductor core losses in the medium frequency range using time response analysis

MACIEJ CHOJOWSKI ¹✉, ROBERT SOSNOWSKI ^{1,2}, MARCIN BASZYŃSKI ¹,
ANDRZEJ STOBIECKI ¹, ROMAN DUDEK ¹, ALEKSANDER DZIADIECKI¹,
CHARALAMBOS KONSTANTINOU ²

¹AGH University of Krakow
Poland

²King Abdullah University of Science and Technology
Saudi Arabia

e-mail: ✉ chojo@agh.edu.pl

(Received: 23.10.2024, revised: 17.04.2025)

Abstract: This paper presents a novel approach for measuring losses in magnetic components intended for medium-frequency power electronic applications. The proposed method enables accurate determination of core losses in power inductors using only voltage and current measurements. Real inductors, consisting of a copper litz winding and low-loss core, are used to test the effectiveness of the method across multiple operating points. The estimation method is able to match the losses with 6.13% accuracy, showing that it is sufficient with only voltage and current measurements, and is efficient in estimating the losses with low overhead.

Key words: core losses, inductor losses analysis, inductor losses determination

1. Introduction

Power electronic systems continue to place greater emphasis on compactness, reduced weight, cost-efficiency, and enhanced performance, especially in active components like transistors, and passive magnetic elements [1–6].

Manufacturers typically provide general information about magnetic material losses in datasheets, mostly based on sinusoidal voltage supply conditions [7–9]. In contemporary hard-switching power electronic systems, magnetic elements are frequently subjected to a square wave voltage input, in contrast to the sinusoidal voltage input assumed by manufacturers in their parameter datasheets [8–13].



© 2025. The Author(s). This is an open-access article distributed under the terms of the Creative Commons Attribution-NonCommercial-NoDerivatives License (CC BY-NC-ND 4.0, <https://creativecommons.org/licenses/by-nc-nd/4.0/>), which permits use, distribution, and reproduction in any medium, provided that the Article is properly cited, the use is non-commercial, and no modifications or adaptations are made.

Conducting measurements in conditions that closely resemble the component's operating environment produces the most reliable results [1, 4, 12, 14]. There are established techniques for measuring losses in magnetic elements, such as electrical measurement methods (voltage and current measurement) [15, 16], or calorimetric methods [17–20]. These methods enable the assessment of overall losses, but it is often necessary to differentiate between core losses and copper losses.

A commonly used approach is the two-winding method, which involves adding a winding to the core of the tested power inductor [21–25]. This additional winding facilitates the measurement of the induced electromotive force (EMF), allowing the calculation of power dissipation in the core. However, the two-winding method is vulnerable to phase discrepancy, which refers to the difference in phase between the measured waveform and the actual inductor current waveform. This discrepancy can arise due to factors such as parasitic inductance of the resistive shunt, probe mismatch, and oscilloscope sampling resolution, and becomes more pronounced at higher waveform frequencies.

Alternative methods for determining core losses eliminate the issue of phase discrepancy but require specialized system solutions [26–29] that alter the operating conditions of the inductor. In [27] and [28], proposed methods for cancelling the reactive voltage of the tested inductor involve the connection of a capacitor or another inductor in series, but precise selection of compensation capacitance or inductance values is critical and challenging. Reactive voltage compensation methods are modified in [2] and [29]. Both methods involving inductive compensation are used for excitation waveforms of any shape. The technique proposed in [26] involves connecting an air inductor with the same winding in series to the tested core inductor while separately measuring the losses of both inductors calorimetrically and assuming that the difference in measured values determines the losses in the core of the tested power inductor.

As mentioned, the two-winding method for measuring core losses requires an additional winding for EMF measurement. However, with the growing popularity of ready-made inductors in power electronic systems, it is often not feasible to add this additional winding. Therefore, it is essential to develop a non-invasive method that accurately determines core and copper losses in an inductor operating under similar conditions to those in the target system, without requiring modification to the inductor or its operating system.

The method proposed in [30] allows measuring core losses without additional winding but with limited accuracy, which was below 30%. Moreover, the method could not be used for every type of power inductor because core estimation was mostly dependent on a current jump.

The measurement method proposed in this paper can determine core and copper losses without changing the power electronic system or the inductor itself. The proposed Adaptive Estimation Method (AEM) relies solely on voltage and current measurements and does not require EMF measurements. A critical aspect of the approach is the requirement of a high-bandwidth and high-accuracy current and voltage probe to minimize implementation errors of the developed algorithm.

The AEM is applicable in cases where the tested inductor is subjected to a rectangular voltage waveform with adjustable amplitude and frequency produced by a power electronics system. Such excitation corresponds to the operating conditions of the inductor that are frequently encountered in practical power electronic systems. The AEM uses a model of inductor along with an adaptive estimation algorithm to determine all model parameters. This applies to the inductor's operation in the linear region of the B-H magnetization curve, taking into consideration the hysteresis loop.

2. General assumptions for tested inductor

The power inductor model shown in Fig. 1 is adopted for this study [31]. The algorithm's major task is to determine the values of the R_w , L_s , L_m and R_c (Fig. 1) inductor model parameters based on the recorded voltage waveform v of the power supply (rectangular bipolar waveform with a fixed duty cycle of 50%) and the inductor current for quasi steady-state i . This model should be characterized by a good representation of the time waveform and total power losses, as well as allowing approximate determination of core losses. The proximity of the turns in the winding creates small capacitances between adjacent turns and the inductor as a whole behaves like a combination of resistive-inductive elements connected in parallel with capacitance. At low frequencies, the self-capacitance has no significant effect but at higher frequencies it could cause the inductor to oscillate. The model shows neglected interturn capacitance C [32] (it is permissible in the frequency range of interest below 200 kHz [33,34]). Figure 2 shows a typical theoretical voltage waveform (a square wave with a frequency of $1/T$) and the current waveform of the inductor.

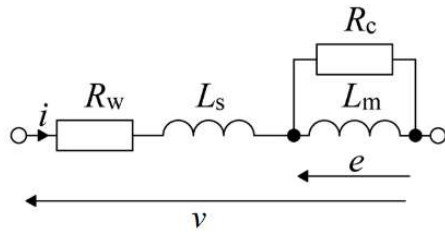


Fig. 1. Inductor model equivalent circuit diagram (the electromotive force is marked as e)

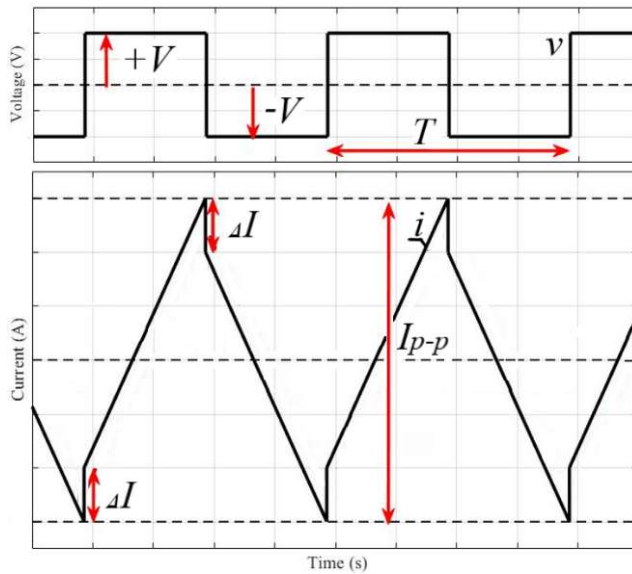


Fig. 2. Illustrative time waveforms of the applied voltage v and inductor current i with current jump ΔI and current peak-to-peak value I_{p-p} , for frequency $f = 1/T$

In order to determine the parameter values of the model in Fig. 1, an optimization method is applied. Based on the measured v and i waveforms, the values of the model parameters are determined, taking into account the constraints on parameter values. Subsequently, a simulation of

the model's operation is carried out with the determined parameter values. The obtained current waveform is compared to the measured waveform, and the quality criterion value is determined. Then, the model parameters are adjusted appropriately, and another simulation is conducted. This process is repeated until the optimal values (in accordance with the adopted quality criterion) of the model parameters are found. The algorithm's proper operation is limited by the following conditions:

- The current jump (carrying information about core losses) is measurable and has a significant value (relative to the current amplitude). The greater the ratio of the time constant $\tau_1 = L_m/R_c$ to the period of the supply voltage (T), the greater the relative value of this jump. Therefore, it is not visible for a very small value of this time ratio ($\tau_1/T \approx 0$).
- The time constant of this jump must be sufficiently small compared to the period of the supply voltage. It is equal to: $\tau_2 = L_s/(R_w + R_c)$. For relatively large values of the ratio of τ_2/T , the simplified $R_w L_m R_c$ model is insufficient to reproduce the current time response (no visible rapid current change) [30].

It must be stated that in a practical inductor the leakage inductance is much smaller than magnetizing inductance $L_s \ll L_m$.

3. Algorithm operation

The waveforms v and i are recorded in a quasi-steady state for a bipolar rectangular voltage with a 50% duty cycle. The data are postprocessed:

1. The time window containing the maximum available number of complete periods of the measured voltage (v) and current (i) is determined.
2. The active power (P), root-mean-square values of voltage (V_{RMS}) and current (I_{RMS}) are calculated for the previously determined complete periods.
3. To achieve a shorter time to reach a quasi-steady state the simulation starts from the moment when the phase shift of the supply voltage is equal to 90° .

The block structure of the algorithm is presented in Fig. 3. The proposed algorithm needs to simulate the virtual inductor model. The first step is to find the initial parameters of the inductor model – inductance L_0 , winding resistance R_w and core resistance R_c . The initial value of the L_0 inductance is estimated using the formula (for bipolar square wave voltage with duty cycle 50%):

$$L_0 = L_m + L_s = \frac{V}{2 \cdot I_{p-p} \cdot f}, \quad (1)$$

where I_{p-p} is the peak-to-peak current and f is the switching frequency.

The active power (P), which represents all losses in the inductor, is calculated as follows:

$$P = \frac{1}{T} \int_{t_0}^{t_0+T} (v \cdot i) dt. \quad (2)$$

The resistance is a non-negative real number $R \geq 0$ with the upper limit selected based on the basic inductor model with a series connection of resistive and inductive elements. In this case, all power losses will be represented by one resistive element.

In the next part, the model is extended to a general inductor model (Fig. 1). The initial core losses are estimated by the method proposed in [30] based on a current jump.

If the value of the current jump (ΔI) is relatively large, it is possible to narrow down the range of checked R_w values by estimating the initial core losses (P_{c0}) [30], e.g., with an assumed accuracy of $\pm 30\%$, which is an upper and lower limit of the algorithm.

$$P_{c0} = \frac{V_{\max} \Delta I}{2} (\pm 30\%). \quad (3)$$

And then the new winding losses estimation range will be:

$$P_{w \min} = P - 1.3 \cdot P_{c0}, \quad (4a)$$

$$P_{w \max} = P - 0.7 \cdot P_{c0}. \quad (4b)$$

If $P_{w \min} < 0$, it is assumed that it equals zero because the active power cannot be lower than 0. If $P_{w \max} > P$, it is assumed that it equals P because winding losses cannot be higher than the summed core and winding losses.

$$R_{w \min} = \frac{P_{w \min}}{I_{\text{RMS}}^2}, \quad (5a)$$

$$R_{w \max} = \frac{P_{w \max}}{I_{\text{RMS}}^2}. \quad (5b)$$

The values of L and R_w are determined iteratively. In each iteration, the ranges of their variability and the number of points considered from this range are determined.

For each pair of determined values L and R_w in the model (Fig. 3), the value of R_c is determined in such a way that the difference between the estimated power loss for the simulation results and the calculated total power loss (core and winding) for the measurement data is close to zero.

The operational steps of the algorithm can be described as follows:

1. Simulations are performed for the given parameters and the applied voltage.
2. For each simulation, the error of the estimated current waveform \hat{i} and the measured current i is calculated: $\tilde{i} = \hat{i} - i$.
3. For each simulation, the average relative fitting error of the estimated current waveform \hat{i} is determined in relation to the measured current i .

$$J = \frac{1}{N} \sum_{n=1}^N \frac{|\tilde{i}|}{|i|}. \quad (6)$$

In general, the algorithm allows achieving similar current shape and same total active power losses in the simulation model of the inductor and in the tested inductor. The information about current jump ΔI during PWM switching allows getting information about core losses.

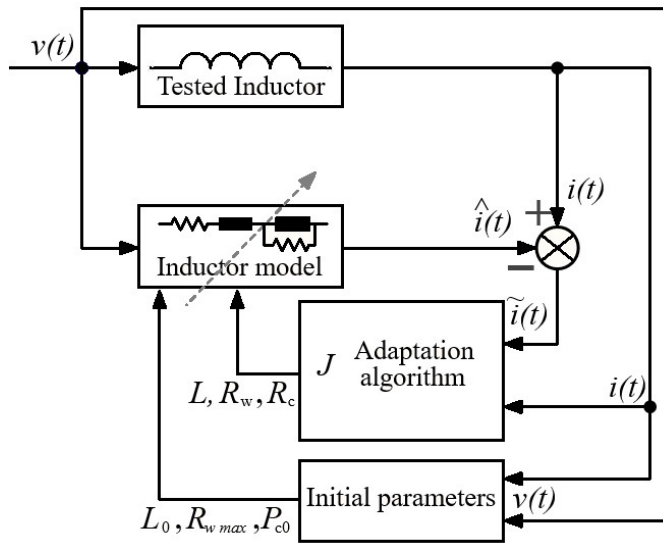


Fig. 3. Block diagram of the proposed adaptive estimation method

4. Experimental results

4.1. Test setup

The proposed method has been used in real power inductor testing. In the first example, the commercial inductor with a litz wire and FINEMET core is tested (Fig. 4). The inductor's mechanical and electrical parameters are listed in Table 1.

Table 1. Mechanical and electrical parameters of the tested power inductor with FINEMET core

Parameter	Value
core type	EC 78/30
weight	~590 g
core dimensions	78 × 74 × 30 mm
gap dimension	2 × 0.1 mm + 1 × 0.15 mm
wire type	2 × (630 × 0.1)
number of turns – main winding (voltage measurement)	8 turns
number of turns – additional winding (EMF measurement)	8 turns
inductance calculated by supplier (unknown method)	90 μH +/− 10%
maximum DC current	35 A
maximum induction	0.675 T

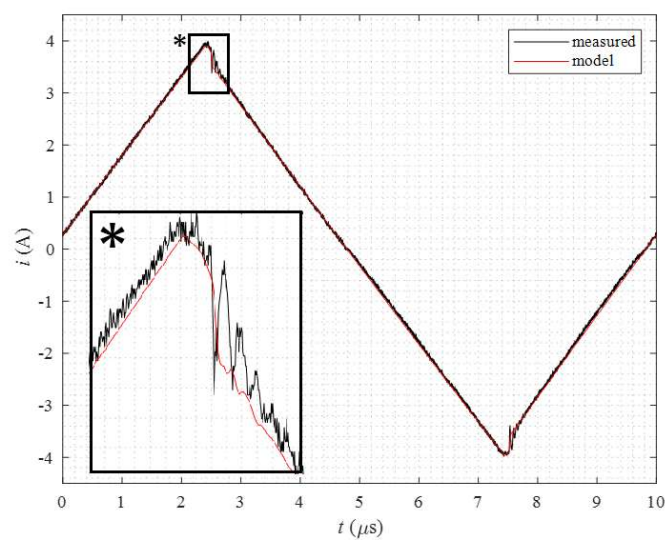


Fig. 5. The measured and simulation current waveforms for a supply voltage frequency equals 100 kHz

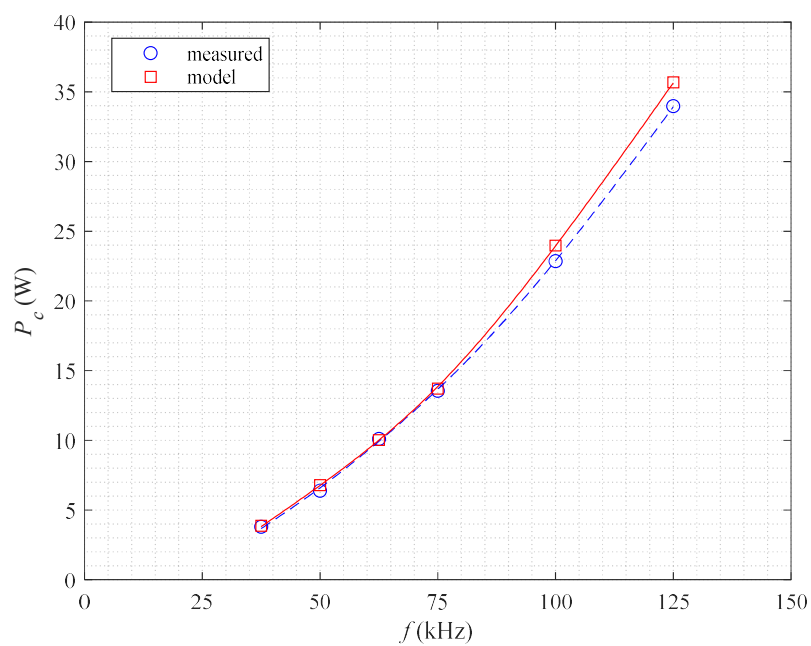


Fig. 6. Core power losses determined based on the measurements (marked as measured) and using the optimized model for different voltage waveform frequency values

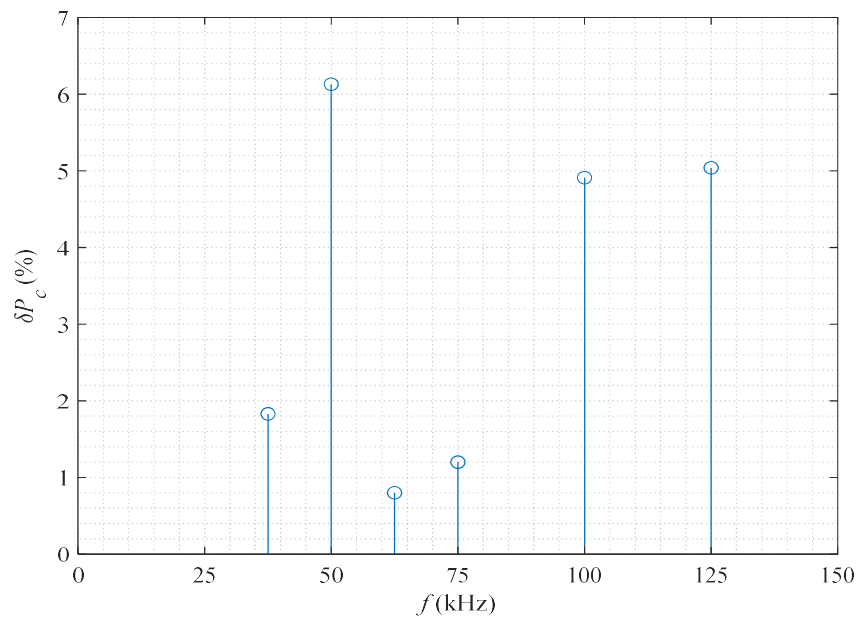


Fig. 7. Relative error of the core power estimation for different frequency values of the voltage waveform

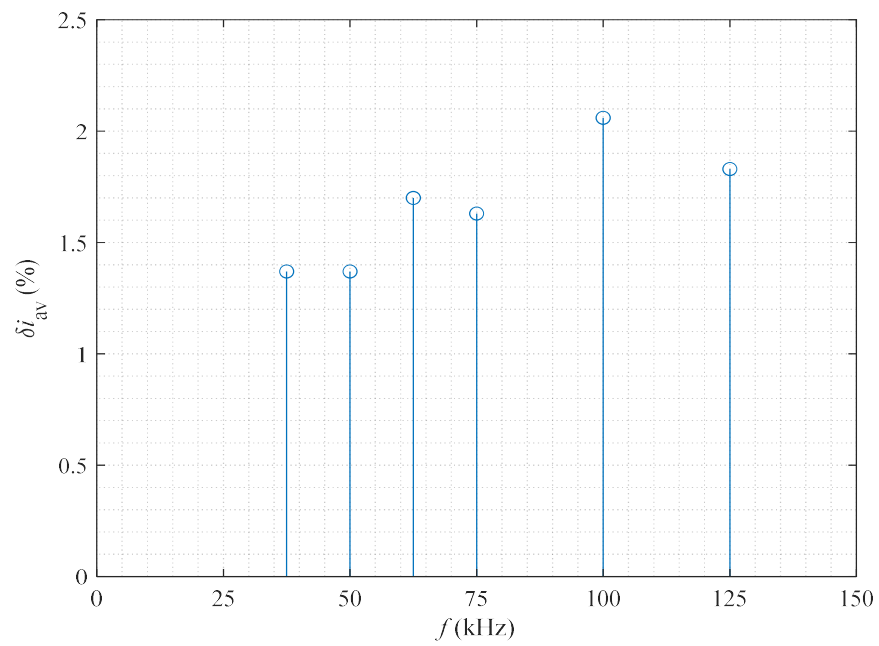


Fig. 8. Relative error of the current fitting for different frequency values of the voltage waveform

Table 2. The results of measurements and simulations using the fitted model for different voltage waveform frequency values

Measurements	f [kHz]	37.5	50.0	62.5	75.0	100.0	125.0
	V_m [V]	40.5	53.5	67.2	79.2	106.0	131.2
	P [W]	4.4	7.8	11.5	15.7	27.4	40.8
	P_c [W]	3.8	6.4	10.1	13.6	22.9	34.0
Fitted parameters	R_w [mΩ]	112.2	195.7	282.6	401.4	695.0	1040.1
	L [μH]	70.4	69.8	69.3	69.6	69.6	69.2
	R_c [Ω]	423.2	421.9	450.3	456.6	467.3	480.0
Model errors	δi_{av} [%]	1.37	1.37	1.70	1.63	2.06	1.83
	δP [%]	0.04	0.01	0.00	0.04	0.02	0.04
	δP_c [%]	1.83	6.13	0.80	1.20	4.91	5.04

4.3. Constant frequency value

Table 3 shows the changes in the inductor losses as a function of the I_{p-p} current parameter while maintaining the constant value of the switching frequency $f = 50$ kHz. Figures 9, 10 and 11 show power losses, the relative difference (%) in the losses calculated and the relative difference for the current response for both methods. It is assumed that the core losses calculated by (7) are the reference method.

Table 3. The results of measurements and simulations using the fitted model for different peak-to-peak current values

Measurements	I_{p-p} [A]	15.3	16.7	18.2	19.6	20.9	22.4	23.8	25.2	26.5
	V_m [V]	109.5	119.5	129.0	138.7	148.5	158.9	169.2	179.3	189.0
	P [W]	36.1	43.3	52.1	59.2	68.2	79.6	89.9	101.9	113.3
	P_c [W]	32.9	39.6	47.2	54.9	63.1	73.0	82.8	92.6	103.4
Fitted parameters	R_w [mΩ]	230.8	232.9	237.4	232.7	233.0	233.5	236.7	240.3	240.8
	L [μH]	72.6	72.6	72.1	71.9	72.0	72.0	72.0	72.2	72.3
	R_c [Ω]	379.6	376.5	364.6	371.1	369.0	362.1	363.4	360.1	359.8
Model errors	δi_{av} [%]	2.23	2.10	1.97	1.93	1.86	1.77	1.74	1.65	1.56
	δP [%]	0.02	0.02	0.04	0.02	0.02	0.02	0.01	0.01	0.01
	δP_c [%]	4.13	4.43	3.36	5.66	5.50	4.64	5.00	3.77	4.08

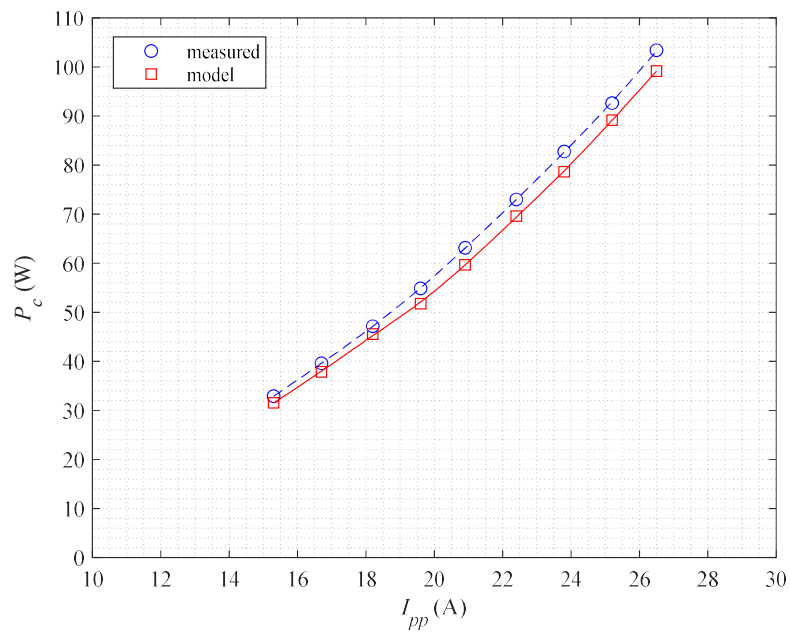


Fig. 9. Core power losses determined based on the measurements (marked as measured) and using the optimized model for different peak-to-peak current values

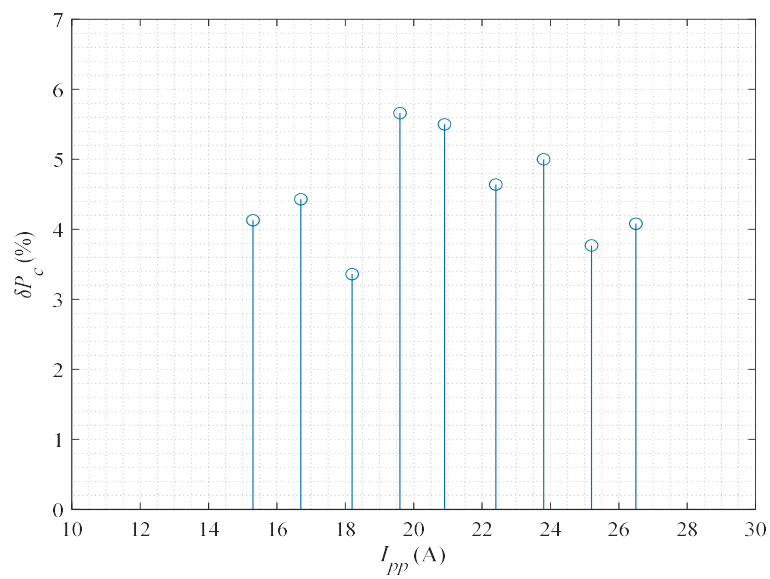


Fig. 10. Relative error of the core power estimation for different peak-to-peak current values

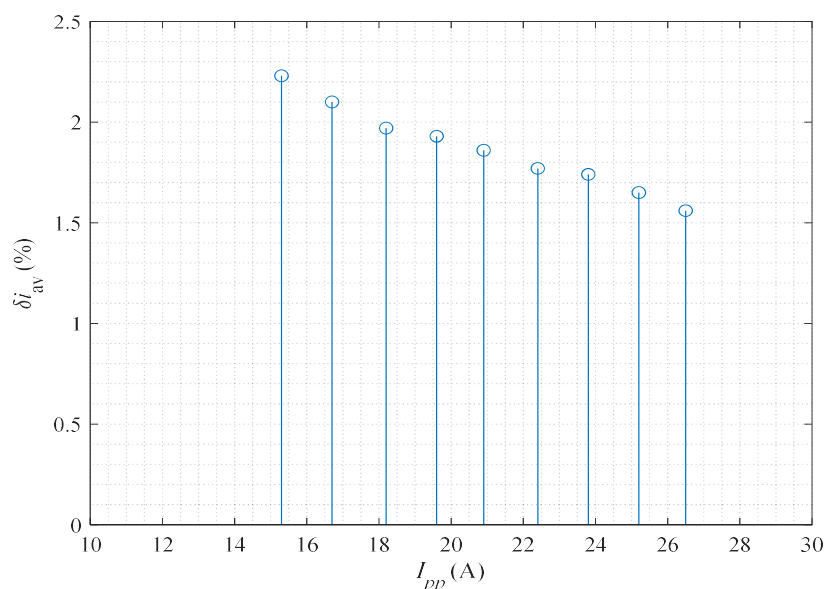


Fig. 11. Relative error of the current fitting for different peak-to-peak current values

5. Conclusions

The presented novel AEM enables the calculation of losses in the inductor core under conditions similar to those found in actual power electronic converters (square voltage power supply). It is important that the tested inductor operates in conditions for which the relationship $T \ll \tau$ is satisfied, which means that for the applied rectangular voltage the corresponding current closely resembles a triangular one. The calculation of inductor core losses using only measurements of current and voltage qualifies as a novel method, provided it offers distinct advantages over existing approaches and demonstrates unique insights.

The AEM enables the separation of losses in the core and the winding, which is confirmed by comparison with the well-known and accurate two-winding method. In most cases the relative difference is below 5% and the maximal error is 6.13%. When the losses are relatively small, measurement errors tend to increase due to challenges in accurately identifying the switching moment and the magnitude of the current jump.

All parameters, resistances, and inductances from Fig. 1, determined using the AEM can be used for precision time or frequency domain simulation purposes.

The method demonstrates a fundamentally new way to interpret voltage and current data that reveals previously inaccessible aspects of core losses.

Acknowledgements

This article was created as part of the “Inicjatywa Doskonałości – Uczelnia Badawcza” project at AGH.

References

- [1] Bahmani A., *Core loss evaluation of high-frequency transformers in high-power DC-DC converters*, Proc. 13th International Conference on Ecological Vehicles and Renewable Energies (EVER), Monte Carlo, Monaco, pp. 1–7 (2018), DOI: [10.1109/EVER.2018.8362341](https://doi.org/10.1109/EVER.2018.8362341).
- [2] Hou D., Mu M., Lee F.C., Li Q., *New high-frequency core loss measurement method with partial cancellation concept*, IEEE Transactions on Power Electronics, vol. 32, no. 4, pp. 2987–2994 (2017), DOI: [10.1109/TPEL.2016.2573273](https://doi.org/10.1109/TPEL.2016.2573273).
- [3] Imaoka J., Yu-Hsin W., Shigematsu K., Aoki T., Noah M., Yamamoto M., *Effects of high-frequency operation on magnetic components in power converters*, Proc. IEEE 12th Energy Conversion Congress Exposition – Asia (ECCE-Asia), Singapore, pp. 978–984 (2021), DOI: [10.1109/ECCE-Asia49820.2021.9479365](https://doi.org/10.1109/ECCE-Asia49820.2021.9479365).
- [4] Mannam R., Gorantla S.R., Vangala N., *A practical technique to measure transformer losses in high frequency SMPS*, SN Applied Sciences, vol. 1, no. 3, 227 (2019), DOI: [10.1007/s42452-019-0239-4](https://doi.org/10.1007/s42452-019-0239-4).
- [5] Rasekh N., Wang J., Yuan X., *A novel in-situ measurement method of high-frequency winding loss in cored inductors with immunity against phase discrepancy error*, IEEE Open Journal of the Industrial Electronics Society, vol. 2, pp. 545–555 (2021), DOI: [10.1109/OJIES.2021.3121088](https://doi.org/10.1109/OJIES.2021.3121088).
- [6] Rodriguez-Sotelo D., Rodriguez-Licea M.A., Araujo-Vargas I., Prado-Olivarez J., Barranco-Gutiérrez A.I., Perez-Pinal F.J., *Power Losses Models for Magnetic Cores: A Review*, Micromachines, vol. 13, no. 3, 418, pp. 1–27 (2022), DOI: [10.3390/mi13030418](https://doi.org/10.3390/mi13030418).
- [7] Wang J., Dagan K.J., Yuan X., Wang W., Mellor P.H., *A practical approach for core loss estimation of a high-current gapped inductor in PWM converters with a user-friendly loss map*, IEEE Transactions on Power Electronics, vol. 34, no. 6, pp. 5697–5710 (2019), DOI: [10.1109/TPEL.2018.2867264](https://doi.org/10.1109/TPEL.2018.2867264).
- [8] Ayachit A., Kazimierczuk M.K., *Steinmetz Equation for Gapped Magnetic Cores*, IEEE Magnetics Letters, vol. 7, pp. 1–4 (2016), DOI: [10.1109/LMAG.2016.2540609](https://doi.org/10.1109/LMAG.2016.2540609).
- [9] Steinmetz C.P., *On the law of hysteresis*, Proceedings of the IEEE, vol. 72, no. 2, pp. 197–221 (1984), DOI: [10.1109/PROC.1984.12842](https://doi.org/10.1109/PROC.1984.12842).
- [10] Matsumori H., Shimizu T., Wang X., Blaabjerg F., *A practical core loss model for filter inductors of power electronic converters*, IEEE Journal of Emerging and Selected Topics in Power Electronics, vol. 6, no. 1, pp. 29–39 (2018), DOI: [10.1109/JESTPE.2017.2761127](https://doi.org/10.1109/JESTPE.2017.2761127).
- [11] Sun H., Li Y., Lin Z., Zhang C., Yue S., *Core loss separation model under square voltage considering DC bias excitation*, AIP Advances, vol. 10, no. 1, 015229 (2020), DOI: [10.1063/1.5131561](https://doi.org/10.1063/1.5131561).
- [12] Yue S., Yang Q., Li Y., Zhang C., Xu G., *Core loss calculation of the soft ferrite cores in high frequency transformer under non-sinusoidal excitations*, Proc. 20th International Conference on Electrical Machines and Systems (ICEMS), Sydney, Australia, pp. 1–5 (2017), DOI: [10.1109/ICEMS.2017.8056411](https://doi.org/10.1109/ICEMS.2017.8056411).
- [13] Barg S., Ammous K., Mejbri H., Ammous A., *An improved empirical formulation for magnetic core losses estimation under nonsinusoidal induction*, IEEE Transactions on Power Electronics, vol. 32, no. 3, pp. 2146–2154 (2017), DOI: [10.1109/TPEL.2016.2555359](https://doi.org/10.1109/TPEL.2016.2555359).
- [14] Yi L., Moon J., *In situ direct magnetic loss measurement with improved accuracy for lossier magnetics*, IEEE Transactions on Instrumentation and Measurement, vol. 71, no. 6001414 (2022), DOI: [10.1109/TIM.2022.3150877](https://doi.org/10.1109/TIM.2022.3150877).
- [15] Liu B., Chen W., Wang J., Chen Q., *A practical inductor loss testing scheme and device with high frequency pulse width modulation excitations*, IEEE Transactions on Industrial Electronics, vol. 68, no. 5, pp. 4457–4467 (2021), DOI: [10.1109/TIE.2020.2984985](https://doi.org/10.1109/TIE.2020.2984985).
- [16] Karthikeyan V., Rajasekar S., Pragaspathy S., Blaabjerg F., *Core loss estimation of magnetic links in DAB converter operated in high-frequency non-sinusoidal flux waveforms*, Proc. IEEE International

- Conference on Power Electronics, Drives and Energy Systems (PEDES), Chennai, India (2018), DOI: [10.1109/PEDES.2018.8707857](https://doi.org/10.1109/PEDES.2018.8707857).
- [17] Grecki F., Drofenik U., *Calorimetric medium frequency loss measurement of the foil inductor winding*, Proc. IEEE 19th International Power Electronics and Motion Control Conference (PEMC), pp. 611–614 (2021), DOI: [10.1109/PEMC48073.2021.9432598](https://doi.org/10.1109/PEMC48073.2021.9432598).
- [18] Jafari A. et al., *Calibration-free calorimeter for sensitive loss measurements: case of high-frequency inductors*, Proc. IEEE 21st Workshop on Control and Modeling for Power Electronics (COMPEL), Aalborg, Denmark (2020), DOI: [10.1109/COMPEL49091.2020.9265756](https://doi.org/10.1109/COMPEL49091.2020.9265756).
- [19] Kleeb T., Dombert B., Araújo S., Zacharias P., *Loss measurement of magnetic components under real application conditions*, Proc. 15th European Conference on Power Electronics and Applications (EPE), Lille, France (2013), DOI: [10.1109/EPE.2013.6631895](https://doi.org/10.1109/EPE.2013.6631895).
- [20] Papamanolis P., Guillod T., Krismer F., Kolar J.W., *Transient calorimetric measurement of ferrite core losses up to 50 MHz*, IEEE Transactions on Power Electronics, vol. 36, no. 3, pp. 2548–2563 (2021), DOI: [10.1109/TPEL.2020.3017043](https://doi.org/10.1109/TPEL.2020.3017043).
- [21] Marin-Hurtado A.J., Rave-Restrepo S., Escobar-Mejía A., *Calculation of core losses in magnetic materials under nonsinusoidal excitation*, Proc. 13th International Conference on Power Electronics (CIEP), Guanajuato, Mexico, pp. 87–91 (2016), DOI: [10.1109/CIEP.2016.7530736](https://doi.org/10.1109/CIEP.2016.7530736).
- [22] Yue S., Yang Q., Li Y., Zhang C., *Core loss calculation for magnetic materials employed in SMPS under rectangular voltage excitations*, AIP Advances, vol. 8, no. 5, 056121 (2018), DOI: [10.1063/1.5007201](https://doi.org/10.1063/1.5007201).
- [23] Zhao H., Eldeeb H.H., Zhang Y., Zhan Y., Xu G., Mohammed O.A., *An improved core loss model of ferromagnetic materials considering high-frequency and non-sinusoidal supply*, IEEE Transactions on Industry Applications, vol. 57, no. 4, pp. 4336–4346 (2020), DOI: [10.1109/IAS44978.2020.9334779](https://doi.org/10.1109/IAS44978.2020.9334779).
- [24] Wang J., Yuan X., Rasekh N., *Triple Pulse Test (TPT) for Characterizing Power Loss in Magnetic Components in Analogous to Double Pulse Test (DPT) for Power Electronics Devices*, Proc. IECON 2020 The 46th Annual Conference of the IEEE Industrial Electronics Society, pp. 4717–4724 (2020), DOI: [10.1109/IECON43393.2020.9255039](https://doi.org/10.1109/IECON43393.2020.9255039).
- [25] Baszyński M., Chojowski M., Dziadecki A., Stobiecki A., Dudek R., Skotniczny J., *A Method and a Three Source Converter for Medium Frequency Magnetic Elements Losses Measurement*, IEEE Transactions on Industrial Electronics, vol. 70, iss. 12 (2023), DOI: [10.1109/TIE.2023.3239874](https://doi.org/10.1109/TIE.2023.3239874).
- [26] Wang W.B., Pansier F., Haan S.D., Ferreira J.A., *Novel and simple calorimetric methods for quantifying losses in magnetic core and GaN transistor in a high frequency boost converter*, Chinese Journal of Electrical Engineering, vol. 2, no. 2, pp. 68–75 (2016), DOI: [10.23919/CJEE.2016.7933128](https://doi.org/10.23919/CJEE.2016.7933128).
- [27] Mu M., Li Q., Gilham D., Lee F.C., Ngo K.D.T., *New core loss measurement method for high frequency magnetic materials*, IEEE Transactions on Power Electronics, vol. 29, no. 8, pp. 4374–4381 (2013), DOI: [10.1109/TPEL.2013.2286830](https://doi.org/10.1109/TPEL.2013.2286830).
- [28] Mu M., Lee F.C., Li Q., Gilham D., Ngo K.D.T., *A high frequency core loss measurement method for arbitrary excitations*, Proc. Appl. Power Electron. Conf. Expo., pp. 157–162 (2011), DOI: [10.1109/APEC.2011.5744590](https://doi.org/10.1109/APEC.2011.5744590).
- [29] Sanusi B.N., Ouyang Z., *Magnetic Core Losses under Square-wave Excitation and DC Bias in High Frequency Regime*, Proc. 2022 IEEE Applied Power Electronics Conference and Exposition (APEC), pp. 633–639 (2022), DOI: [10.1109/APEC43599.2022.9773563](https://doi.org/10.1109/APEC43599.2022.9773563).
- [30] Chojowski M., Baszyński M., Dziadecki A., Dudek R., Stobiecki A., *Time Domain Analysis for Measuring Core Losses in Inductive Elements for Power Electronics: An Investigation Study*, IEEE Access (2023), DOI: [10.1109/ACCESS.2023.3312544](https://doi.org/10.1109/ACCESS.2023.3312544).

- [31] Li Z., Han W., Xin Z., Liu Q., Chen J., Loh P.C., *A Review of Magnetic Core Materials, Core Loss Modeling and Measurements in High-Power High-Frequency Transformers*, CPSS Transactions on Power Electronics and Applications, vol. 7, no. 4, pp. 359–373 (2022), DOI: [10.24295/CPSSSTPEA.2022.00033](https://doi.org/10.24295/CPSSSTPEA.2022.00033).
- [32] Pasko S.W., Kazimierczuk M.K., Grzesik B., *Self-Capacitance of Coupled Toroidal Inductors for EMI Filters*, IEEE Transactions on Electromagnetic Compatibility, vol. 57, iss. 2, pp. 216–223 (2015), DOI: [10.1109/TEMC.2014.2378535](https://doi.org/10.1109/TEMC.2014.2378535).
- [33] Javidi F.N., Nymand M., *A New Method for Measuring Winding AC Resistance of High-Efficiency Power Inductors*, IEEE Transactions on Power Electronics, vol. 33, iss. 12, pp. 10736–10747 (2018), DOI: [10.1109/TPEL.2018.2805867](https://doi.org/10.1109/TPEL.2018.2805867).
- [34] Kazimierczuk M.K., *High-Frequency Magnetic Components*, 2nd Edition, Wiley (2014), DOI: [10.1002/9781118717806](https://doi.org/10.1002/9781118717806).